



This paper is a part of the hereunder thematic dossier published in OGST Journal, Vol. 68, No. 6, pp. 951-1113 and available online [here](#)

Cet article fait partie du dossier thématique ci-dessous publié dans la revue OGST, Vol. 68, n°6, pp. 951-1113 et téléchargeable [ici](#)

DOSSIER Edited by/Sous la direction de : **C. Barrère-Tricca**

IFP Energies nouvelles International Conference / Les Rencontres Scientifiques d'IFP Energies nouvelles
MAPI 2012: Multiscale Approaches for Process Innovation
MAPI 2012 : Approches multi-échelles pour l'innovation des procédés

Oil & Gas Science and Technology – Rev. IFP Energies nouvelles, Vol. 68 (2013), No. 6, pp. 951-1113

Copyright © 2013, IFP Energies nouvelles

- 951 >Editorial
- 977 >*Molecular Simulation of Adsorption in Microporous Materials*
Modélisation moléculaire de l'adsorption dans les solides microporeux
M. Yannourakou, P. Ungerer, B. Leblanc, X. Rozanska, P. Saxe, S. Vidal-Gilbert, F. Gouth and F. Montel
- 995 >*Sulfur Deactivation of NO_x Storage Catalysts: A Multiscale Modeling Approach*
Empoisonnement des matériaux de stockage des NO_x par le soufre : approche multi-échelles
N. Rankovic, C. Chizallet, A. Nicolle, D. Berthout and P. Da Costa
- 1007 >*From Detailed Description of Chemical Reacting Carbon Particles to Subgrid Models for CFD*
De la description détaillée des particules de carbone chimiquement réactives aux modèles de sous-maille pour la CFD
S. Schulze, M. Kestel, P.A. Nikrityuk and D. Safronov
- 1027 >*Development of a General Modelling Methodology for Vacuum Residue Hydroconversion*
Développement d'une méthodologie générale de modélisation pour l'hydroconversion de résidu sous vide
L. Pereira de Oliveira, J.J. Verstraete and M. Kolb
- 1039 >*A General Approach for Kinetic Modeling of Solid-Gas Reactions at Reactor Scale: Application to Kaolinite Dehydroxylation*
Une approche générale de la modélisation cinétique des réactions solide-gaz à l'échelle du réacteur : application à la déshydroxylation de la kaolinite
L. Favergeon, J. Morandini, M. Pijolat and M. Soustelle
- 1049 >*A Multiscale Approach for Modeling Oxygen Production by Adsorption*
Modélisation de la production d'oxygène par adsorption par une approche multi-échelle
D. Pavone and J. Roesler
- 1059 >*Bubbles in Non-Newtonian Fluids: A Multiscale Modeling*
Bulles en fluide non newtonien : une approche multi-échelle
X. Frank, J.-C. Charpentier, F. Cannevière, N. Midoux and H.Z. Li
- 1073 >*Multiscale Study of Reactive Dense Fluidized Bed for FCC Regenerator*
Étude multi-échelle d'un lit fluidisé dense réactif de type régénérateur FCC
G. Moula, W. Nastoll, O. Simonin and R. Andreux
- 1093 >*CO₂ Capture Cost Reduction: Use of a Multiscale Simulations Strategy for a Multiscale Issue*
Réduction du coût du captage de CO₂ : mise en œuvre d'une stratégie de simulations multi-échelle pour un problème multi-échelles
L. Raynal, A. Gomez, B. Caillat and Y. Haroun
- 1109 >*International Conference on Multiscale Approaches for Process Innovation – MAPI – 25-27 January 2012 – Round Table Discussion*
Conférence internationale sur les approches multi-échelles pour l'innovation des procédés – MAPI – 25-27 janvier 2012 – Comptes-rendus des discussions de la table-ronde
H. Toulhoat

A General Approach for Kinetic Modeling of Solid-Gas Reactions at Reactor Scale: Application to Kaolinite Dehydroxylation

L. Favergeon^{1*}, J. Morandini², M. Pijolat¹, M. Soustelle¹

¹ Centre SPIN, École Nationale Supérieure des Mines, 158 cours Fauriel, 42023 Saint-Étienne - France

² Astek Rhône-Alpes, 1 place du verseau, 38130 Échirolles - France

e-mail: favergeon@emse.fr - jmorandini@astek.fr - mpijolat@emse.fr - msoustelle@emse.fr

* Corresponding author

Résumé — Une approche générale de la modélisation cinétique des réactions solide-gaz à l'échelle du réacteur : application à la déshydroxylation de la kaolinite — La compréhension du comportement de réacteurs industriels est difficile dans le cas de réactions solide-gaz. En effet la phase solide est un milieu granulaire dans lequel circulent des réactifs et des produits gazeux. Les propriétés d'un tel milieu sont modifiées dans l'espace et le temps en raison des réactions se produisant à une échelle microscopique. Les conditions thermodynamiques sont fixées non seulement par les conditions de fonctionnement du réacteur, mais aussi par la chaleur et les transferts de matière dans le réacteur. Nous proposons de résoudre numériquement les équations thermohydrauliques en les combinant avec les lois cinétiques qui décrivent les réactions hétérogènes. L'avantage majeur de cette approche est la grande variété des modèles cinétiques de transformation de grains disponibles (~40) comparée à l'approche habituelle, particulièrement dans le cas de germination en surface suivie de la croissance des germes. En effet, ce type de modèle doit permettre de décrire quantitativement la cinétique à l'échelle microscopique du grain, en fonction de la fréquence surfacique de germination et de la réactivité surfacique de croissance obtenues lors d'expériences isothermes et isobares. Les termes sources de chaleur et de matière entrant dans les bilans à l'échelle macroscopique dépendent de la cinétique à l'échelle microscopique. La résolution de ces équations permet d'obtenir la température et les pressions partielles dans le réacteur, qui à leur tour influencent le comportement cinétique.

Abstract — A General Approach for Kinetic Modeling of Solid-Gas Reactions at Reactor Scale: Application to Kaolinite Dehydroxylation — Understanding the industrial reactors behavior is a difficult task in the case of solid state reactions such as solid-gas reactions. Indeed the solid phase is a granular medium through which circulate gaseous reactants and products. The properties of such a medium are modified in space and time due to reactions occurring at a microscopic scale. The thermodynamic conditions are driven not only by the operating conditions but also by the heat and mass transfers in the reactor. We propose to numerically resolve the thermohydraulic equations combined with kinetic laws which describe the heterogeneous reactions. The major advantage of this approach is due to the large variety of kinetic models of grains transformation (~40) compared to the usual approach, especially in the case of surface nucleation and growth processes which need to quantitatively describe the grain conversion kinetics at a microscopic scale due to nucleation frequency and growth rate laws obtained in separate isothermal and isobaric experiments. The heat and mass transfers terms entering in the balance equations at a macroscopic scale depend on the kinetics evaluated at the microscopic scale. These equations give the temperature and partial pressure in the reactor, which in turn influence the microscopic kinetic behavior.

NOTATIONS

| | |
|-----------------|---|
| α | Fractional conversion of the powder |
| β | Fractional conversion of a grain |
| C | Concentration (mol.m^{-3}) |
| c_p | Heat capacity at constant pressure ($\text{J.kg}^{-1}.\text{K}^{-1}$) |
| D | Diffusivity ($\text{m}^2.\text{s}^{-1}$) |
| D_{ij} | Multicomponent diffusion coefficient ($\text{m}^2.\text{s}^{-1}$) |
| S_m | Space function ($\text{m}^2.\text{mol}^{-1}$) |
| ε | Porous medium porosity |
| ε_0 | Initial porous medium porosity |
| ε_r | Emissivity |
| ϕ | Areic reactivity of growth ($\text{mol.m}^{-2}.\text{s}^{-1}$) |
| g | Acceleration of gravity (m.s^{-2}) |
| γ | Areic frequency of nucleation ($\text{nuclei.m}^{-2}.\text{s}^{-1}$) |
| h | Heat transfer coefficient ($\text{W.m}^{-2}.\text{K}^{-1}$) |
| H | Hydrodynamic charge (m) |
| J^D | Diffusion flow vector ($\text{mol.m}^{-2}.\text{s}^{-1}$) |
| k | Thermal conductivity ($\text{W.m}^{-1}.\text{K}^{-1}$) |
| k_p | Diffusion coefficient ($\text{m}^2.\text{Pa}^{-1}.\text{s}^{-1}$) |
| K | Darcy's permeability (m^2) |
| M_i | Molar mass for constituent i (kg.mol^{-1}) |
| η | Dynamic viscosity of the fluid (Pa.s) |
| P | Total pressure (Pa) |
| P_i | Partial pressure of reactive gas (Pa) |
| Q_T | Heat sources density (W.m^{-3}) |
| Q_C | Concentration sources density ($\text{mol.m}^{-3}.\text{s}^{-1}$) |
| R | Ideal gas constant ($= 8.314 \text{ J.K}^{-1}.\text{mol}^{-1}$) |
| r_0 | Initial radius of the grain (m) |
| ρ | Density (kg.m^{-3}) |
| σ | Stefan Boltzmann constant ($\text{W.m}^{-2}.\text{K}^{-4}$) |
| T | Temperature (K) |
| T_a | Ambient temperature (K) |
| u | Rate vector (m.s^{-1}) |
| u_d | Flowing rate vector ($\text{m}^2.\text{s}^{-1}$) |
| u_n | Incoming flow density (m.s^{-1}) |
| V_{mA} | Molar volume of A ($\text{m}^3.\text{mol}^{-1}$) |

INTRODUCTION

Solid-gas reactions are of great interest in many industrial fields such as nuclear, chemistry, metallurgy, CO_2 capture, etc. Industrial reactors in which these reactions take place are difficult to quantitatively describe. Indeed the solid phase is a granular medium through which circulate gaseous reactants and products. The properties of such a medium are modified in space and time due to reactions occurring at a microscopic scale. The thermodynamic conditions are driven not only by the operating conditions but also by the heat and mass transfers in the reactor. Several models have been developed to account for the complexity of these transformations such as the grain model [1], the pore model [2] and related

incremented models. However most of these models are based on the law of additive reaction times first used by Sohn [3] for which the order respective to the gas in the kinetic rate equation must be equal to 1. However such condition is scarcely encountered in many gas-solid reactions, which may results in erroneous results.

Moreover, such approaches necessitate to describe the reaction kinetics using the shrinking core model or similar laws, so that the rate follows Equation (1):

$$\frac{d\alpha}{dt} = A \exp\left(-\frac{E}{RT}\right) f(\alpha) \quad (1)$$

in which α is the fractional conversion, A is a pre-exponential term, E is the apparent activation energy and $f(\alpha)$ a mathematical function which depends of the kind of model of transformation. About ten different $f(\alpha)$ are available from the literature data [4, 5]. However such an equation implies very restrictive assumptions that make them suitable in many cases either due to the Arrhenius temperature dependence term or due to nucleation and growth competition [6].

We thus use a more general approach for kinetic modeling, including the previous models and models based on surface-nucleation and growth processes (anisotropic or isotropic growth) for the three usual symmetries (spheres, cylinders, planes) and other possible kinetic assumptions depending of where the rate-determining step occurs and the sense of development of the new phase. We propose [6] a large variety of models at the microscopic scale based on a general equation of the reaction rate which accounts for the real influence of the partial pressures P_i of the relevant gases:

$$\frac{d\alpha}{dt} = \phi(T, P_i, \dots) S_m(t, \phi, \gamma, r_0) \quad (2)$$

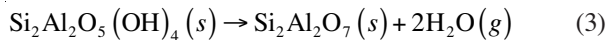
where $\phi(T, P_i, \dots)$ is the areic reactivity of growth, function of the thermodynamic conditions only (temperature, partial pressure, etc.) and $S_m(t, \phi, \gamma, r_0)$ is a function of the initial and current morphology of the sample and therefore of time, of ϕ , of the areic frequency of nucleation γ and of the grains dimensions (e.g. r_0 is the radius for spherical grain).

Using Equation (2), about forty kinetic models may be derived based on various assumptions on the nucleation and growth processes in order to simulate heterogeneous reactions. These models can be simulated using CIN3 software (No. IDD N FR001130014.000.SP.2009.000.30625).

Nevertheless CIN3 is able to simulate reactions if the temperature and the partial pressures of the gases involved in the reaction are uniform inside the granular medium (even if these uniform temperature and partial pressure evolve during the transformation), so it is not adapted for modeling large amounts of solid sample. Indeed in the case of real industrial heterogeneous reactors, the situation is much more difficult to simulate than the case of a reaction with a very small amount of solid sample. In fact, the medium properties are modified by chemical reactions occurring at a microscopic scale.

The thermodynamic conditions are driven not only by operating conditions but also by mass and heat transfers inside the granular medium. In order to overcome such problems, we have developed a multi-physic approach based on the finite elements method which combines the resolution of the thermohydraulic equations with the kinetic laws describing the heterogeneous reactions at the scale of dense particles. This is the aim of the multi-physic software CIN4.

In order to validate CIN4, we have chosen to study the influence of the powder bed thickness in the case of the dehydroxylation of kaolinite according to the reaction:



This reaction has well been studied in the past and many authors [7-13] agree that the rate-determining step of growth is a diffusion step.

Section 1 presents the experimental procedures for characterizing the kaolinite powder and for obtaining kinetic curves. Experimental results are also given. Section 2 presents the various scales approach and the main assumptions made in CIN4. Then, Section 3 and 4 summarize a simplified presentation of the different mathematical and numerical models used, for kinetic modeling at grains scale as well as for heat and mass transfers at reactor scale. Finally, Section 5 presents the results of CIN4 simulations for the dehydroxylation reaction at the reactor scale (*i.e.* the thermobalance) with different heights of the powder bed in the crucible.

1 EXPERIMENTAL: METHODS AND RESULTS

The sample under investigation was obtained from AGS. The BET surface area of this material was determined by means of a Micromeritics ASAP 2010 apparatus using the nitrogen adsorption isotherm at 77 K. It was found equal to $24.2 \text{ m}^2 \cdot \text{g}^{-1}$.

Scanning electron microscopy (JEOL JSM-840) of the initial material is shown in Figure 1. The individual particles are hexagonal-shaped platelets, their mean radius size r_0 being around $0.15 \mu\text{m}$. By approximating the thickness h to $0.05 \mu\text{m}$, the calculated surface area is equal to $25.7 \text{ m}^2 \cdot \text{g}^{-1}$ (with a volumic mass of $2.65 \text{ g} \cdot \text{cm}^{-3}$) which is in agreement with the BET measurement.

The dehydroxylation of kaolinite was followed by means of a SETARAM TAG16 balance. Isothermal and isobaric curves were obtained by heating the studied kaolinite in an alumina crucible (2 cm height, 1 cm diameter) at different temperatures in the range 420-460°C under water vapor pressure fixed at 2.5 hPa, 7 hPa, 10 hPa, 15 hPa and 20 hPa by means of SETARAM WETSYS. The sample was first heated at 100°C under vacuum ($<10^{-3}$ hPa) for water degassing then water vapor was introduced and the sample was heated at the desired temperature with a heating rate of $30^\circ\text{C} \cdot \text{min}^{-1}$. In consequence, the first part of the curves is not in isothermal condition since temperature increased from

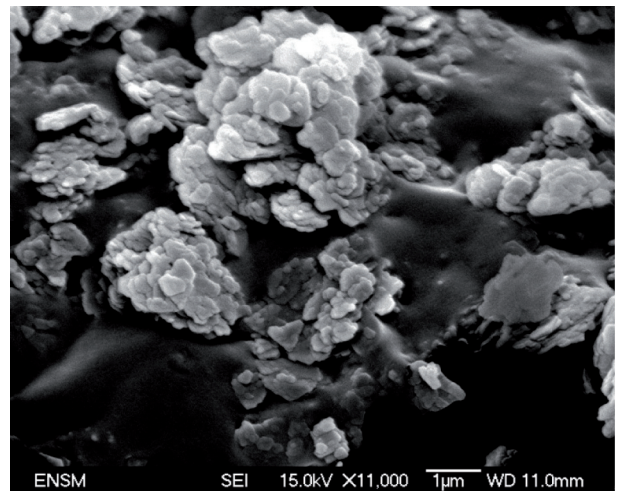


Figure 1
SEM picture of the kaolinite.

100°C to the operating condition. This non-isothermal part represents a value of the fractional conversion in the range 0.06-0.10 depending on the operating temperature.

A first series of experiments was performed with about 25 mg of powder. During the entire transformation, the sample weight was low enough to prevent any effect of pressure gradients in the powder layer. Figure 2 shows the rate curves $d\alpha/dt(\alpha)$ obtained in isothermal and isobaric conditions for different temperatures under $P(\text{H}_2\text{O}) = 7 \text{ hPa}$ (Fig. 2a) and different water vapor pressure at $T = 450^\circ\text{C}$ (Fig. 2b). As expected, the reaction rate increases with temperature and decreases with water vapor pressure.

The second series of experiments was done with various heights of the powder bed. In the same crucible as previously, two distinct TGA experiments were performed at 450°C under a water vapor pressure of 7 hPa: the first one with 50 mg of powder corresponding to a powder bed height of 3 mm; the second one with 300 mg corresponding to 10 mm. The kinetic curves and rates curves obtained with both bed heights are presented in Figure 3. One can see that the powder bed height has an important effect on the kinetic curves since the maximum reaction rate obtained for 3 mm is about twice more that obtained with 10 mm (and is about twice less than that obtained with 1 mm – see Fig. 2).

2 GENERAL PRESENTATION OF THE MODELING

2.1 The Scales for Modeling

Various geometrical scales characterize all phenomena which occur in a reactor. A rigorous description of our modeling process requires a precise definition of these different scales. We have deliberately set these scales from the objects: mesh,

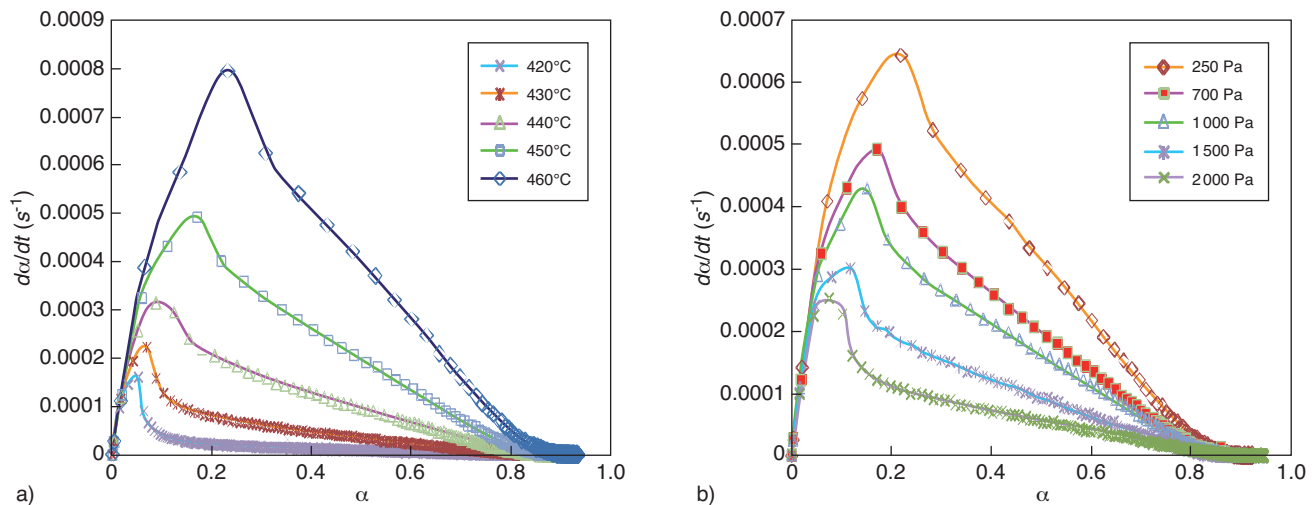


Figure 2

Reaction rate *versus* fractional conversion for the dehydroxylation of kaolinite. a) Influence of temperature ($P(\text{H}_2\text{O})$ 7 hPa); b) influence of water partial pressure ($T = 450^\circ\text{C}$).

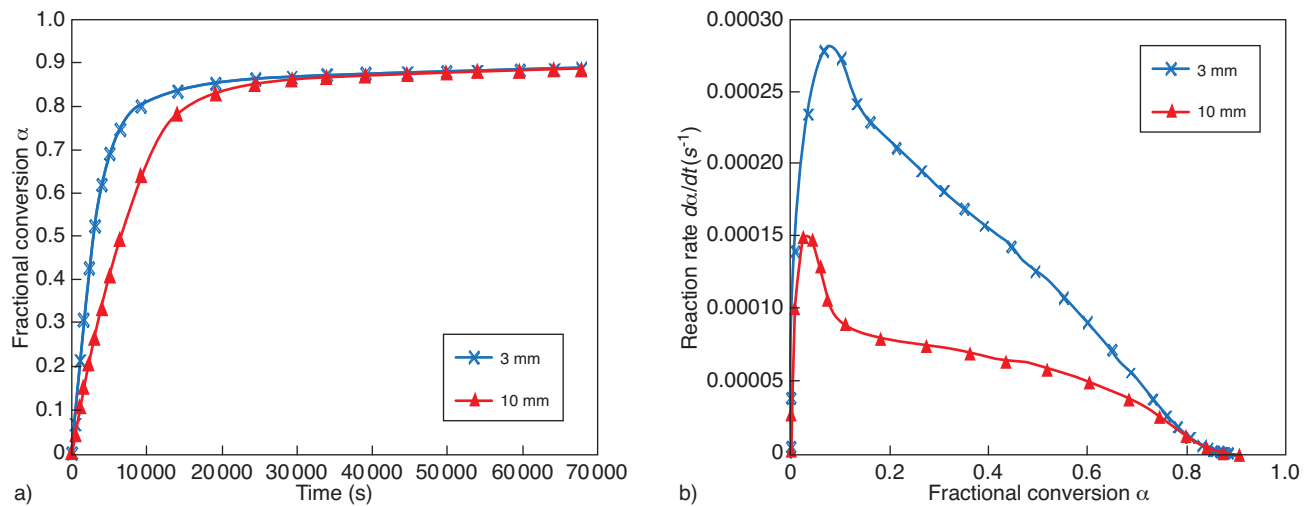


Figure 3

a) Kinetic curves; b) rate curves for kaolinite dehydroxylation ($T = 450^\circ\text{C}$, $P(\text{H}_2\text{O}) = 7$ hPa) obtained for 3-mm and 10-mm bed heights.

grain, grains population, agglomerate and reactor. In this paper, only three scales will be discussed: grain, grain population and reactor. At the grain scale, the nuclei appear at the grain surface¹ and grow at the expense of the initial solid phase: the kinetic rate depends of the shape of the grain, the type of growth, the localization of the rate limiting-step of growth, the direction of development of the new phase. Then, a microscopic population is a set of grains in the same thermodynamic conditions, *i.e.* the gradients of temperature and gas partial pressure are extremely small inside the population. When the nucleation process is concomitant to

(1) Avrami's laws cannot be used for solid-gas heterogeneous reactions involving powders since they are based on bulk nucleation in an infinite volume, which is not physically acceptable.

the growth one, statistical considerations allow to define average behavior of this population from grain's one. Finally at the reactor scale, the chemical reaction is coupled with mass and heat transfers.

2.2 The Assumptions of the Model

Six assumptions are done in this model:

- A1: the gas production and consumption by the reaction do not disturb the total pressure spatial distribution;
- A2: the gases are diluted in a carrier gas;
- A3: the gas flow rates are low (less than 5 L.h⁻¹ for a diameter of 2 cm);

- A4: the gases are considered as ideal;
- A5: the growth process can be described by a succession of elementary steps, one of them controls the growth kinetics (rate-determining step approximation);
- A6: the grains shape and the size distribution are known.

3 MATHEMATICAL MODELING

3.1 Kinetic Laws at Grain and Microscopic Population Scale

As previously recalled, in order to model reactions which involve surface nucleation and growth of the nuclei, one can use Equation (1). For isothermal and isobaric conditions, the S_m function can take various expressions calculated from assumptions on the growth type (isotropic or anisotropic), the development direction of the new phase (inwards or outwards), the localization of the rate determining step of growth and the grains shape (spheres, cylinders, plates). Soustelle [14] detailed the laws establishment and the expressions of S_m for each model.

In the software CIN4 about forty kinetic models of heterogeneous reactions are available. Some of these models are derived at grain scale: in this case, nucleation is considered as instantaneous compared to growth, so all the grains take the same kinetic law. Other models are derived at microscopic population scale: both nucleation and growth are taken into account, which leads to two kinds of models. According to the growth type (isotropic or anisotropic), two methods are used to calculate the fractional conversion of the reaction:

- in the case of isotropic growth of the nuclei, we used a statistical approach based on the works of Johnson and Mehl [15] and Mampel [16], then of Delmon [17];
- in the case of anisotropic growth, each grain starts its transformation at various times and the whole microscopic fractional conversion can be obtained considering the nuclei appearing on each grain of the microscopic population [18].

Moreover, CIN4 enables to consider a grain size distribution which is much more realistic than a single grain size.

3.2 Heat and Mass Transport at Reactor Scale

The macroscopic scale is the center of heat and mass exchanges that are described by the thermal and hydrodynamic models, as well as by a mass transfer equation.

3.2.1 Thermal Model

Heat transfer is described by the following equation valid throughout each part of the reactor Ω^T :

$$\left[(1-\varepsilon)\rho_s c_{ps} + \varepsilon\rho_g c_{pg} \right] \frac{\partial T}{\partial t} + \varepsilon\rho_g c_{pg} \vec{u} \cdot \vec{\nabla} T + \vec{\nabla} \cdot (-k\vec{\nabla} T) = Q^T \quad (4)$$

where s and g indexes refer to solids and gases respectively.

This equation is accompanied by two kinds of boundary conditions:

- Neumann conditions which impose the value of the heat flow on $\partial\Omega_N^T$ boundary:

$$-k\vec{\nabla} T \cdot \vec{n} = \phi_{imposed} + h(T - T_a) + \varepsilon_r \sigma (T^4 - T_a^4) \quad (5)$$

- Dirichlet conditions which impose the value of the temperature on $\partial\Omega_D^T$ boundary:

$$T = T_D \quad (6)$$

These equations are valid for each part of the reactor: solid ($\varepsilon = 0$), gas ($\varepsilon = 1$), porous media ($0 < \varepsilon < 1$).

3.2.2 Hydrodynamic Model

As the granular medium is static and as we consider solid-gas reactions, mass transfers are only due to the flowing of the gas produced or consumed inside the porous medium. The modeling of this flow inside the porous medium is based on notions of hydrodynamic charge and flow rate considerations. Hydrodynamic charge is calculated according to:

$$H = z + \frac{P}{\rho g} + \frac{1}{2g} u^2 \quad (7)$$

The flow rate is not the rate of fluidic particles inside the pores but an equivalent continuous rate. This flow rate is linked to the mass gradient according to the Darcy's law, which is expressed by:

$$\vec{u}_d = -\frac{K}{\eta} \vec{\nabla}(\rho g h) \approx -\frac{K}{\eta} \vec{\nabla} P = -k_p \vec{\nabla} P \quad (8)$$

The whole pressure field (or charge) is solution of a conservation equation. Neglecting source terms due to gas production and consumption (reaction is slow compared to the gas flow), the hydrodynamic problem can be written as:

$$\vec{\nabla} \cdot (-k_p \vec{\nabla} P) = 0 \quad (9)$$

with the boundary conditions: $-k_p \vec{\nabla} P \cdot \vec{n} = -u_n$ on $\partial\Omega_N^T$ and $P = P_D$ on $\partial\Omega_D^T$.

3.2.3 Mass Transport

Gas phase is governed by the ideal gas law. Thus the total molar concentration inside the gas is equal to $C = \frac{P_r}{RT}$. The molar convective flow is due to the transport by the gas displacement and is expressed by:

$$\vec{J}_i^c = C\vec{u} = -\frac{P_r}{RT} \vec{u} \quad (10)$$

Diffusion in porous media is a complex phenomenon including diffusion flow, Knudsen diffusion, Soret effect,

which is well explained by Reid *et al.* [19]. Here, only the diffusion flow is taking into account:

$$\vec{J}_i^D = -D_{ij}^D \vec{\nabla} C_j = -\frac{D_{ij}^D}{RT} \vec{\nabla} P_j \quad (11)$$

and finally each partial pressure is solution of the following equation:

$$\frac{\varepsilon}{RT} \frac{\partial P_i}{\partial t} + \frac{\varepsilon}{RT} \vec{u}_d \cdot \vec{\nabla} P_i - \vec{\nabla} \cdot \left(\frac{D_{ij}^D}{RT} \vec{\nabla} P_j \right) = Q_i^C \quad (12)$$

with the boundary conditions:

$$-\frac{D_{ij}^D}{T} \vec{\nabla} P_j \cdot \vec{n} = R\phi_i \text{ on } \partial\Omega_N^T \text{ and } P_i = P_{iD} \text{ on } \partial\Omega_D^T.$$

3.3 Coupling Between the Microscopic Population Scale and the Reactor Scale

At the microscopic scale, the reaction fractional conversion is evaluated for a representative population of grains. By finite difference it is possible to derive the reaction rate $\frac{d\alpha}{dt}$, which in turn allows to calculate the heat and mass sources produced by the reaction. Thus the heat source density is equal to:

$$Q^T = \sum_{i=1}^{n_g} \nu_i M_A \frac{1-\varepsilon}{V_{mA}} \frac{d\alpha}{dt} \Delta H_i \quad (13)$$

and the mass (partial pressure) source density for a gas i is equal to:

$$Q_i^C = \nu_i \frac{1-\varepsilon}{V_{mA}} \frac{d\alpha}{dt} \quad (14)$$

So, due to these sources terms, the chemical reaction at the microscopic scale impacts the spatial and temporal evolution of the thermodynamic processes at the reactor scale. Inversely since temperature and partial pressure change modify the areic frequency of nucleation and the areic reactivity of growth, thermodynamic influences fractional conversion of the microscopic reaction. It is worthwhile to notice that CIN4 allows to simulate the behavior of reactions for which the kinetic rate at time t (at the microscopic population scale) depends on the local thermodynamic conditions that were established between $t = 0$ and t . CIN4 highly improves the previous approaches which were limited to kinetic model based at grain scale only, excluding models based on competing surface nucleation and growth processes. The equations used in CIN4 require numerous physical properties (porosity, viscosity, density, heat capacity, thermal conductivity, diffusivity). CIN4's user should be able to calculate these properties using empirical laws or mathematical models like for example those given by Bird *et al.* [20].

4 NUMERICAL MODELING

At grain and microscopic population scales, two types of modeling are possible according to the type of growth:

anisotropic or isotropic. In the first case, the method allows to calculate the change of the fractional conversion *versus* time for all grains in each granulometric class. When the growth is isotropic, we used the Mampel's method [16] for three possible grain shapes: spheres, cylinders and plates. At reactor scale, for each Equation (4), (9) and (12) (*i.e.* heat, hydrodynamic and mass transport problems), two finite element formulations were built, depending on the system symmetry (cylindrical or cartesian coordinates). A classical way is followed to obtain weak formulations for each state variable: temperature, hydrodynamic charge and partial pressures.

5 APPLICATION TO THE DEHYDROXYLATION OF KAOLINITE

5.1 Kinetic Modeling at the Grains Population Scale

In order to interpret the experimental curves obtained with thin powder beds (*Fig. 2*), we used a model involving random nucleation followed by anisotropic growth of the nuclei [18]. Nucleation is supposed to occur at the surface of the individual particles with an areic frequency (γ). Once a nucleus has been formed, the anisotropy of growth is such that the particle is instantaneously covered with a very thin layer of solid product. In this case, the tangential component of the growth rate is very high compared to its radial component. This model was proposed for the dehydroxylation of kaolinite few years ago [12, 13]. In the following, the particles will be considered as flat cylinders, as suggested by the micrography shown in Figure 1, with a mean radius r_0 equal to 0.15 μm and a thickness h equal to 0.05 μm . The rate-determining step is a diffusion step through the metakaolinite already present in the periphery of the particle. Moreover the growth of the metakaolinite is considered as occurring toward the center of the grain. With these assumptions and by considering the volumic expansion coefficient equal to 1 [12] (*i.e.* kaolinite and metakaolinite have the same molar volume $V_{mA} = 97.3 \times 10^{-6} \text{ m}^3 \cdot \text{mol}^{-1}$), the reaction rate $d\alpha/dt$ for the powder can be determined by solving the following equations system [18]:

$$\frac{d\alpha}{dt} = \frac{4\pi h \gamma \phi V_{mA} l_0}{r_0} \int_{\xi}^t \exp(-2\pi h r_0 \gamma \tau) \cdot \ln(1-\beta) d\tau \quad (15)$$

with β the fractional conversion for a single grain born at time τ , solution of the equation:

$$(1-\beta)[\text{Ln}(1-\beta)-1] + 1 = 4 \frac{\phi V_{mA} l_0}{r_0^2} (t-\tau) \quad (16)$$

where l_0 is an arbitrary length, that we choose equal to one.

CIN4 offers the possibility of fitting experimental data obtained at fixed temperature and partial pressures of gases by seeking for the best values of γ and ϕ due to an optimization procedure.

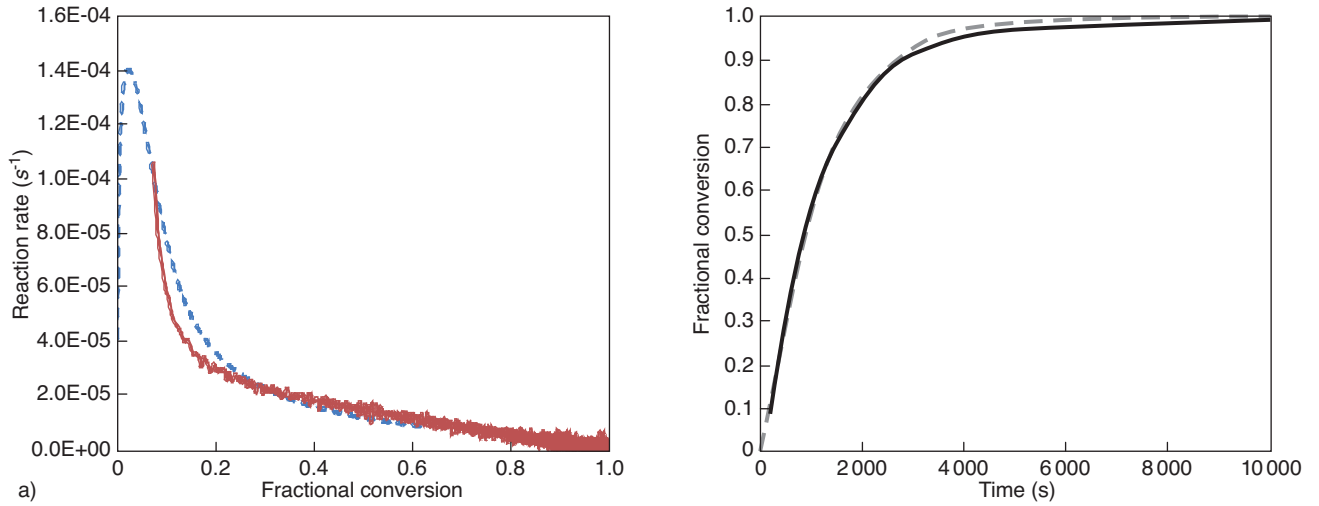


Figure 4

Results of the optimization procedure: comparison of experimental (full line) and calculated curves (dotted line) for a) rate curves at 420°C, $P(\text{H}_2\text{O}) = 7$ hPa; b) kinetic curves at 460°C, $P(\text{H}_2\text{O}) = 7$ hPa.

For γ and ϕ , a range of values is explored. The optimization procedure calculates the rate of reaction for each couple (γ, ϕ) in these ranges and for each of these calculated curves a deviation from the experimental one is calculated by the least square method. The couple (γ, ϕ) for which the deviation is the lowest is kept. The ranges around this couple are then narrowed and the procedure is done again until obtain the lowest deviation between calculated and experimental curves.

These two parameters are both only ones to be adjusted with regard to the experimental curves. Values of γ and ϕ have been looked for using the isothermal part of the experimental curves. Figure 4 shows the results of this optimization procedure at 420 and 460°C ($P(\text{H}_2\text{O}) = 7$ hPa). The values of γ and ϕ obtained for each temperature and each partial pressure allow to determine the laws of variation of γ (in $\text{nb nuclei}\cdot\text{m}^{-2}\cdot\text{s}^{-1}$) and ϕ (in $\text{mol}\cdot\text{m}^{-2}\cdot\text{s}^{-1}$) with T (in Kelvin) and $P(\text{H}_2\text{O})$:

$$\gamma = 10^{26} e^{-0.049T} \left(1 - \frac{P}{P_{eq}}\right)^{3/2} \quad (17)$$

$$\phi = 2 \times 10^{-49} e^{0.1353T} \left(1 - \frac{P}{P_{eq}}\right)^{1/2} \quad (18)$$

5.2 Kinetic Modeling at the Reactor Scale

The second part of modeling concerns the results obtained with thick powder beds. Indeed in such cases, at a given moment, all the dense grains are not in the same conditions

of temperature and partial pressure. It is thus necessary to model the whole reactor taking account the heat and mass transfers.

The first step consists in defining the domain of calculation. The system being axi-symmetric, we have used weak forms written in cylindrical coordinates. Figure 5 shows the mesh used for solving heat and mass transfers' equations throughout the reactor by the finite elements method (the mesh was done by using Gmsh freeware [21]).

There are three areic regions in this mesh: the granular medium (constituted by kaolinite and gas), the alumina crucible and the zone of free gas (He/H₂O mixture). We consider also the following boundary conditions:

- on the incoming boundary, the temperature, flow and composition (He/H₂O mixture) of the entering gaseous mixture is fixed;
- on the outgoing boundary: free for the temperature, total pressure imposed at 1 atm;
- on the sidewall: the boundary is adiabatic and is impassable for the mass flow;
- on the symmetry axis: the radial derivatives of all physical values are equal to 0.

For each areic region, the physical properties were calculated from those of the pure phase. For example, the thermal conductivity k of the granular medium is calculated as follow:

$$k = (1 - \varepsilon)k_s + \varepsilon k_g \quad (19)$$

where ε is the porosity of the granular medium, k_s the thermal conductivity of kaolinite and k_g the thermal conductivity of the gas mixture.

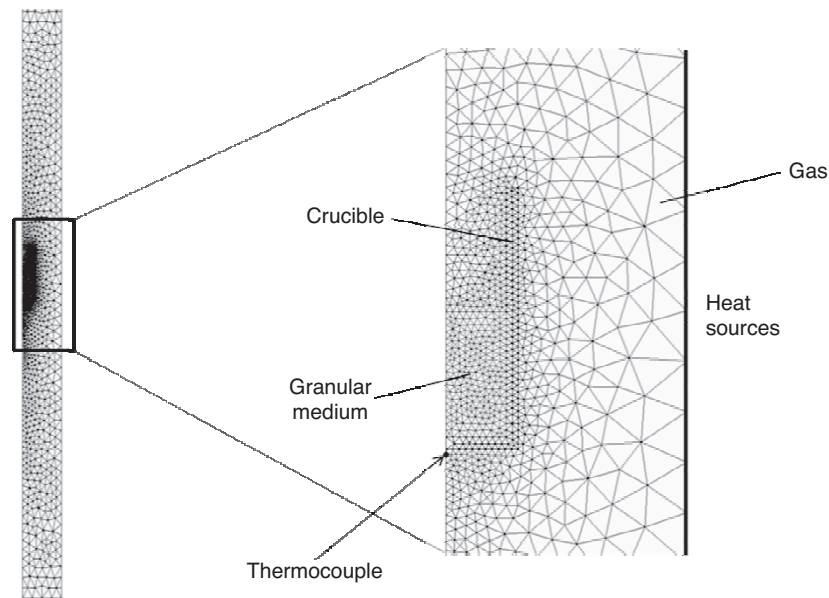


Figure 5

Mesh of a thermobalance containing the crucible and a 10 mm-height powder bed.

The viscosity of the gas mixture is calculated using the semi-empirical formula of Wilke [22]:

$$\eta_{mixture} = \frac{x_{He}\eta_{He} + x_{H_2O}\eta_{H_2O}}{x_{He}\phi_{He/H_2O} + x_{H_2O}\phi_{H_2O/He}} \quad (20)$$

with:

$$\phi_{ij} = \frac{1}{\sqrt{8}} \left[1 + \frac{M_i}{M_j} \right]^{-1/2} \left[1 + \left(\frac{\eta_i}{\eta_j} \right)^{1/2} \left(\frac{M_i}{M_j} \right)^{1/4} \right]^2 \quad (21)$$

M_i the molar mass of species i , η_i the viscosity of species i , x_i the molar fraction of species i .

Inside the granular medium, heat and mass sources are calculated simulating the reaction phenomena at the microscopic level. Figure 6 shows the gas flow rate obtained as well as temperature and fractional conversion fields at a given time for bed heights of 3 and 10 mm, respectively. Figure 7 presents a comparison of the whole rate of reaction *versus* fractional conversion between the experimental data and the simulation for both bed heights.

Figure 7 shows that the simulation is able to discriminate the height of the powder bed from 3 to 10 mm. It is important to notice that these results at reactor scale are obtained by means of numerical simulation without any adjustment of parameters.

Nevertheless the calculated curves are not perfectly superimposed with the experimental ones. Some improvements should be done in order to get better simulations. For example, several points could be improved:

- at the grain scale, the Particles Size Distribution (PSD) can be taken into account to obtain more precise values of γ and ϕ . Indeed Johnson and Kessler [23] and Ortega *et al.* [24] have pointed out the fact that PSD has an impact on the shape of the kinetic curves and should be considered to determine properly kinetic constants in the case of dehydroxylation of kaolinite. This importance of PSD on kinetic modeling has also been underlined by several authors [25, 26] or from a theoretical point of view [27-34];
- at the reactor scale, the change in the physical properties of the granular medium (including the porosity) due to the transformation of kaolinite into metakaolinite should be considered. It could be done by writing a function of the physical properties of the granular medium *versus* fractional conversion.

CONCLUSION

This work presents a general approach for kinetic modeling of heterogeneous reactions by coupling kinetic models at grain and microscopic population scales with both heat and mass transfers by means of the finite element method. The software CIN4 includes kinetic models based on general concepts representative enough of the physical reality; about forty models of chemical transformation of powders are available depending on the shape of the grains, the growth type (isotropic or anisotropic), the development direction of the new phase and the localization of the rate determining step of growth (internal

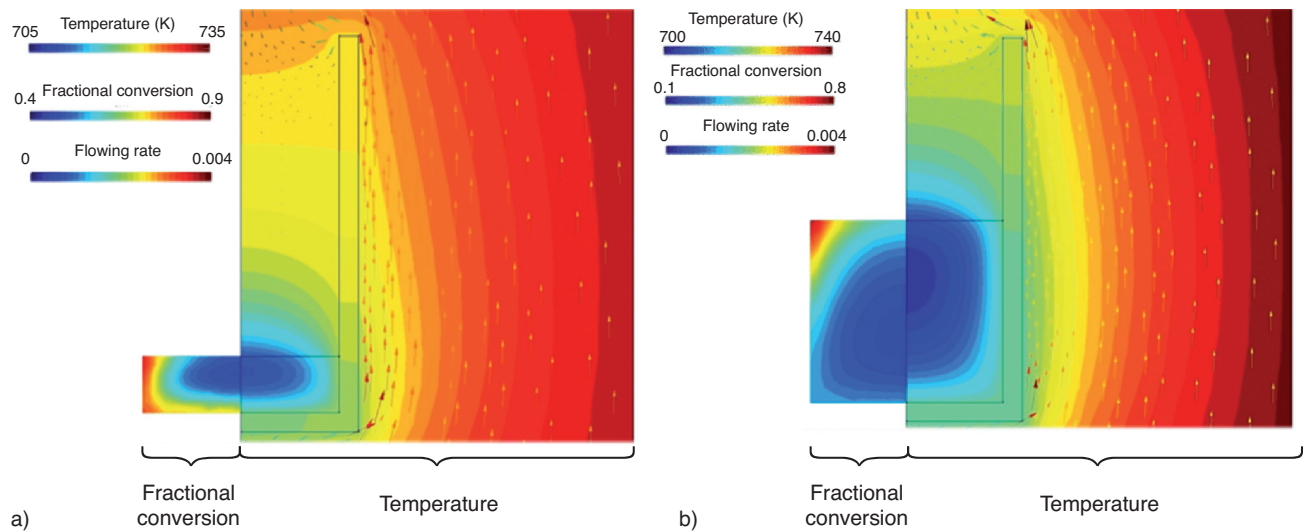


Figure 6

Representation of the temperature field, the fractional conversion and the flowing rate (arrows) at a given time for a) 3 mm-height bed; b) 10 mm-height bed.

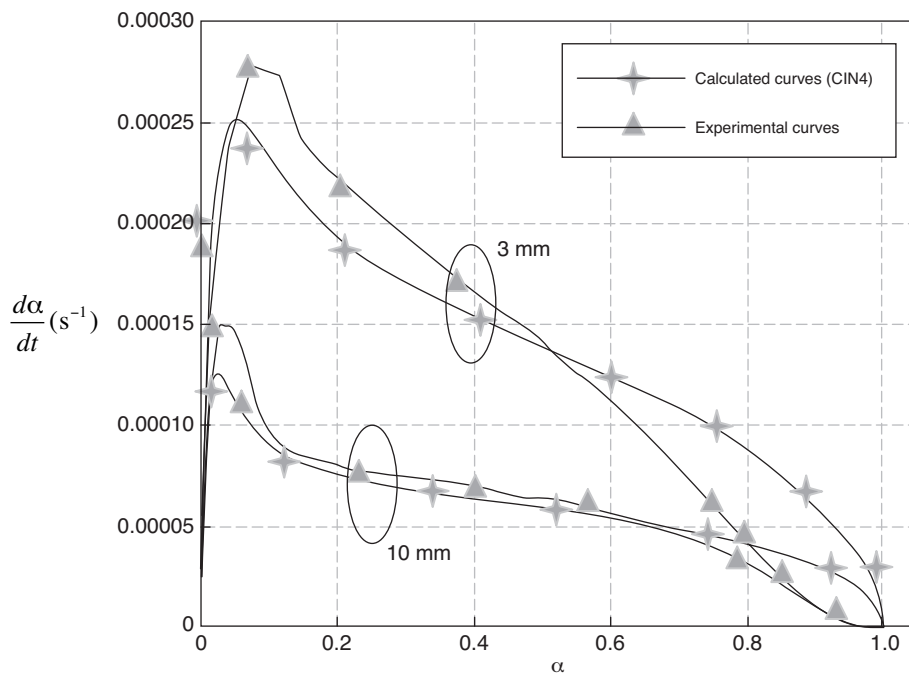


Figure 7

Reaction rate *versus* fractional conversion from the experiment and from the simulation for both powder bed heights.

interface, external interface or diffusion volume). Among these models, 21 include surface nucleation and growth processes. Heat and mass transfers are governed by differential equations and solved by a finite element method. This modeling process allows to simulate not only thermobalances but also industrial reactors. An example of results obtained with CIN4 was presented showing the

influence of the powder bed height on the rate curves for the dehydroxylation of kaolinite.

ACKNOWLEDGMENTS

The authors want to acknowledge Sandra Jacquier for her help on experimental data acquisition.

REFERENCES

- 1 Szekely J., Evans J.W. (1970) A structural model for gas-solid reactions with a moving boundary, *Chem. Eng. Sci.* **25**, 1091-1107.
- 2 Bhatia S., Perlmutter D.D. (1980) A random pore model for fluid-solid reactions: 1. Isothermal, kinetics control, *AIChE J.* **26**, 379-386.
- 3 Sohn H.Y. (1978) The law of additive reaction times in fluid-solid reactions, *Metall. Trans. B* **9**, 89-96.
- 4 Galwey A.K., Brown M.E. (1999) *Thermal decomposition of ionic solids*, Elsevier.
- 5 Sharp J.H., Brindley G.W., Achar B.N.N. (1966) Numerical data for some commonly used solid state reaction equations, *J. Am. Ceram. Soc.* **49**, 379-382.
- 6 Pijolat M., Favergeon L., Soustelle M. (2011) From the drawbacks of “Arrhenius-f(α)” rate equation towards a more general formalism and new kinetic models for the kinetic analysis of solid-gas reactions, *Thermochim. Acta* **525**, 1-2, 93-102.
- 7 Achar B.N.N., Brindley G.W., Sharp J.H. (1966) Kinetics and mechanism of dehydroxylation processes. III. Applications and limitations of dynamic models, in *Proceedings of International Clay Conference*, Jerusalem, vol. 1, pp. 67-73.
- 8 Holt J.B., Cutler I.B., Wadsworth M.E. (1962) Thermal dehydration of kaolinite in vacuum, *J. Am. Ceram. Soc.* **45**, 133-136.
- 9 Brindley G.W., Sharp J.H., Paterson J.H., Achar B.N.N. (1967) Kinetics and mechanism of dehydroxylation processes, I. Temperature and vapor pressure dependence of dehydroxylation of kaolinite, *Am. Mineral.* **52**, 201-209.
- 10 Horvath I. (1985) Kinetics and compensation effect in kaolinite dehydroxylation, *Thermochim. Acta* **85**, 193-198.
- 11 Redfern S.A.T. (1987) The kinetics of dehydroxylation of kaolinite, *Clay Miner.* **22**, 447-546.
- 12 Perrin S. (2002) *PhD Thesis*, École Nationale Supérieure des Mines, Saint-Étienne, France.
- 13 Nahdi K., Perrin S., Pijolat M., Rouquerol F., Ariguib N., Ayadi M. (2002) Nucleation and anisotropic growth model for isothermal kaolinite dehydroxylation under controlled water vapour pressure, *Phys. Chem. Chem. Phys.* **4**, 1972-1977.
- 14 Soustelle M. (2010) *Handbook of Heterogeneous Chemistry*, Edition J. Wiley and ISTE Ltd.
- 15 Johnson W.A., Mehl R.F. (1939) Reaction kinetics in processes of nucleation and growth, *Trans. AIME* **135**, 416-442.
- 16 Mampel K.L. (1940) Zeitzumsatzformeln für heterogene Reaktionen an Phasengrenzen fester Körper, *Z. Phys. Chem. A* **187**, 235-249.
- 17 Delmon B. (1969) *Introduction à la cinétique hétérogène*, Ed. Technip, p. 397.
- 18 Favergeon L., Pijolat M., Soustelle M., A family of surface nucleation and anisotropic growth models for solid-gas reactions, submitted to *Thermochimica Acta*.
- 19 Reid R.C., Prausnitz J.M., Poling B.E. (1987) *The properties of gases and liquids*, McGraw Hill, New-York.
- 20 Bird R.B., Stewart W.E., Lightfoot E.N. (2002) *Transport phenomena*, Wiley International Edition.
- 21 Geuzaine C., Remacle J.F. (2009) Gmsh: a three-dimensional finite element mesh generator with built-in pre- and post-processing facilities, *Int. J. Numer. Methods Eng.* **79**, 11, 1309-1331.
- 22 Wilke C.R. (1950) A viscosity equation for gas mixtures, *J. Chem. Phys.* **18**, 517-519.
- 23 Johnson H.B., Kessler F. (1969) Kaolinite dehydroxylation kinetics, *J. Am. Ceram. Soc.* **52**, 4, 199-204.
- 24 Ortega A., Macias M., Gotor F.J. (2010) The multistep nature of the kaolinite dehydroxylation: kinetics and mechanism, *J. Am. Ceram. Soc.* **1**, 197-203.
- 25 Hutchinson R.W., Kleinberg S., Stein F.P. (1973) Effect of particle-size distribution on the thermal decomposition of a-lead azide, *J. Phys. Chem.* **77**, 7, 870-875.
- 26 Bircumshaw L.L., Newman B.H. (1954) The thermal decomposition of ammonium perchlorate II. The kinetics of the decomposition, the effect of particle size and discussion of results, *Proc. Roy. Soc. A* **227**, 1169, 228-241.
- 27 Sasaki H. (1964) Introduction of particle-size distribution into kinetics of solid-state reaction, *J. Am. Ceram. Soc.* **47**, 10, 512-516.
- 28 McIlvried H.G., Massoth F.E. (1973) Effect of particle size distribution on gas-solid reaction kinetics for spherical particles, *Ind. Eng. Chem. Fund.* **12**, 2, 225-229.
- 29 Kapur P.C. (1973) Kinetics of solid-state reactions of particulate ensembles with size distributions, *J. Am. Ceram. Soc.* **56**, 2, 79-81.
- 30 Lahiri A.K. (1980) The effect of particle size distribution on TG, *Thermochim. Acta* **40**, 289-295.
- 31 Miyokawa K., Masuda I. (1985) Influence of particle size distribution of a sample on the kinetic parameters determined by thermogravimetric curves, *Thermochim. Acta* **86**, 113-118.
- 32 Urrutia G.A., Blesa M.A. (1988) The influence of particle size distribution on the conversion/time profiles under contracting-geometry kinetic regimes, *React. Solids* **6**, 281-284.
- 33 Koga N., Criado J.M. (1997) Influence of the particle size distribution on the CRTA curves for the solid-state reactions of interface shrinkage type, *J. Therm. Anal. Calorim.* **49**, 1477-1484.
- 34 Koga N., Criado J.M. (1998) Kinetic analyses of solid-state reactions with a particle size distribution, *J. Am. Ceram. Soc.* **81**, 11, 2901-2909.

Final manuscript received in May 2012
Published online in May 2013

Copyright © 2013 IFP Energies nouvelles

Permission to make digital or hard copies of part or all of this work for personal or classroom use is granted without fee provided that copies are not made or distributed for profit or commercial advantage and that copies bear this notice and the full citation on the first page. Copyrights for components of this work owned by others than IFP Energies nouvelles must be honored. Abstracting with credit is permitted. To copy otherwise, to republish, to post on servers, or to redistribute to lists, requires prior specific permission and/or a fee: Request permission from Information Mission, IFP Energies nouvelles, fax. +33 1 47 52 70 96, or revueogst@ifpen.fr.